arXiv:1606.01565v3 [cond-mat.mes-hall] 24 Dec 2016

Breaking of Galilean invariance in the hydrodynamic formulation of ferromagnetic thin films

Ezio Iacocca,[1,2,*] T. J. Silva,[3] and Mark A. Hoefer[1]

[1] *Department of Applied Mathematics, University of Colorado, Boulder, Colorado 80309-0526, USA*

[2] *Department of Physics, Division for Theoretical Physics, Chalmers University of Technology, 412 96, Gothenburg, Sweden*

[3] *National Institute of Standards and Technology, Boulder, Colorado 80305-3328, USA*[†]

Abstract

Microwave magnetodynamics in ferromagnets are often studied in the small-amplitude or weakly nonlinear regime corresponding to modulations of a well-defined magnetic state. However, strongly nonlinear regimes, where the aforementioned approximations are not applicable, have become experimentally accessible. By re-interpreting the governing Landau-Lifshitz equation of motion, we derive an exact set of equations of dispersive hydrodynamic form that are amenable to analytical study even when full nonlinearity and exchange dispersion are included. The resulting equations are shown to, in general, break Galilean invariance. A magnetic Mach number is obtained as a function of static and moving reference frames. The simplest class of solutions are termed uniform hydrodynamic states (UHSs), which exhibit fluid-like behavior including laminar flow at subsonic speeds and the formation of a Mach cone and wave-fronts at supersonic speeds. A regime of modulational instability is also possible, where the UHS is violently unstable. The hydrodynamic interpretation opens up novel possibilities in magnetic research.

* E-mail: ezio.iacocca@colorado.edu; Videos of micromagnetic simulations here.

† Contribution of the National Institute of Standards and Technology; not subject to copyright in the United States.

Magnetodynamics in thin film ferromagnets have been studied for many decades. Advances in nanofabrication and the advent of spin transfer [1, 2] and spin-orbit torques [3] have opened a new frontier of experimentally accessible nonlinear physics [4–8]. Large-amplitude excitations negate the use of typical linear or weakly nonlinear analyses [9–11], necessitating instead either micromagnetic simulations [12] or analytical approaches suited to strongly nonlinear dynamics. Therefore, an interpretation of the Landau-Lifshitz (LL) equation that includes full nonlinearity, yet is amenable to analytical study, would be insightful.

A hydrodynamic interpretation was proposed by Halperin and Hohenberg [13] to describe spin waves in anisotropic ferro- and antiferromagnets. Recently, theoretical studies of thin film ferromagnets with planar anisotropy have identified a relationship to superfluid-like hydrodynamic equations [14–19] supporting large-amplitude modes beyond strongly nonlinear spin wave and macrospin modes [10, 11]. However, these studies are limited to the long-wavelength, low-frequency regime where linear and weakly-nonlinear approaches apply. The relaxation of these approximations along with the identification of a deep connection between magnetodynamics and fluid dynamics brings new perspectives on magnetism and reveals novel physical regimes. Indeed, nonlinear, dispersive physics are required to describe superfluids and exotic structures such as solitons, quantized vortices, and dispersive shock waves (DSWs) [20–23], as exemplified by Bose-Einstein condensates (BECs) [20–22, 24–34]. To obtain an analytical description of large-amplitude magnetic textures, we introduce dispersive hydrodynamic (DH) equations for a thin-film ferromagnet.

This letter shows that the LL equation exactly maps into a DH system of equations, without long-wavelength and low-frequency restrictions. The conservative equations map to the Euler equations of a compressible, isentropic fluid. The DH equations for a planar ferromagnet admit spin-current-carrying, spatially periodic magnetization textures termed "uniform hydrodynamic states" (UHSs), providing a continuous and generalized description of spin superflows [14–16] up to small-amplitude spin waves. Within the DH formulation, we prove that planar ferromagnets break Galilean invariance and elucidate their reference-frame-dependent dynamics by identifying the linear dispersion relation for spin waves propagating on top of a UHS background. Such symmetry breaking at the level of linear spin waves is striking and fundamentally different from the non-trivial reference-frame-dependent dynamics of topological textures due to their inherent nonlinearity, e.g., Walker breakdown for domain wall propagation [35] and core reversal in magnetic vortices [36]. In this letter,

we also show that static textures can break Galilean invariance for infinitesimal spin wave excitations that ride on a textured background. To emphasize this novel result, we suggest a Brillouin light scattering experimental test where broken Galilean invariance manifests itself as a spin-wave dispersion shift in the presence of a UHS.

We consider the nondimensionalized LL equation (see Supplementary Material [37])

$$\frac{\partial \mathbf{m}}{\partial t} = -\mathbf{m} \times \mathbf{h}_{\text{eff}} - \alpha \mathbf{m} \times \mathbf{m} \times \mathbf{h}_{\text{eff}}. \tag{1}$$

Damping is parametrized by the Gilbert constant α, $\mathbf{m} = \mathbf{M}/M_s = (m_x, m_y, m_z)$ is the magnetization vector normalized to the saturation magnetization, and $\mathbf{h}_{\text{eff}} = \Delta\mathbf{m} - \sigma m_z \hat{\mathbf{z}} + h_0 \hat{\mathbf{z}}$ is the normalized effective field including: ferromagnetic exchange, $\Delta\mathbf{m}$; total anisotropy determined by $\sigma = \text{sgn}(M_s - H_k)$, where H_k is the perpendicular magnetic anisotropy field, such that $\sigma = +1$ ($\sigma = -1$) represents a material with easy-plane (perpendicular magnetic) anisotropy; and a perpendicular applied field, h_0. This nondimensionalization of a two-dimensional (2D) thin film provides a parameter-free description of materials with planar or uniaxial anisotropy. We consider an idealized case where in-plane magnetic anisotropy is negligible, i.e., its symmetry-breaking contribution only perturbs the leading order solution, similar to domain wall Brownian motion [38].

Fluid-like variables are introduced using the canonical Hamiltonian cylindrical transformation [39]

$$n = m_z, \quad \mathbf{u} = -\nabla\Phi = -\nabla \left[\arctan\left(m_y/m_x\right)\right], \tag{2}$$

where Φ is the azimuthal phase angle. We identify n ($|n| \leq 1$) as the *longitudinal spin density* and $\mathbf{u}$ as the *fluid velocity*. There are two important features of Eq. (2). First, the flow is irrotational because the velocity originates from a phase gradient, i.e., only quantized circulation, such as a magnetic vortex [15], is possible. Second, Φ is undefined when $n = \pm 1$, corresponding to fluid *vacuum*.

Utilizing the transformation (2) and standard vector calculus identities, the LL equa-

tion (1) can be exactly recast as two DH equations [37]

$$\frac{\partial n}{\partial t} = \nabla \cdot \underbrace{\left[(1-n^2)\mathbf{u}\right]}_{\text{spin current}} + \underbrace{\alpha(1-n^2)\frac{\partial \Phi}{\partial t}}_{\text{spin relaxation}}, \tag{3a}$$

$$\frac{\partial \mathbf{u}}{\partial t} = \nabla \underbrace{\left[(\sigma - |\mathbf{u}|^2)n\right]}_{\text{velocity flux}} - \underbrace{\nabla\left[\frac{\Delta n}{1-n^2} + \frac{n|\nabla n|^2}{(1-n^2)^2}\right]}_{\text{dispersion}} \tag{3b}$$

$$\underbrace{-\nabla h_0}_{\text{potential force}} + \underbrace{\alpha\nabla\left[\frac{1}{1-n^2}\nabla\cdot\left[(1-n^2)\mathbf{u}\right]\right]}_{\text{viscous loss}}.$$

Equation (3a) is reminiscent of spin density continuity [40] from which we identify the spin density flux as the spin current

$$\mathbf{J}_s = -(1-n^2)\mathbf{u}. \tag{4}$$

Vacuum carries zero spin current. However, maximal spin current is reached when $n = 0$, identified as the *saturation density*. This implies that ferromagnetic textures ($\mathbf{u} \neq 0$) are better spin current conductors than small-amplitude spin waves [41]. The hydrodynamic equivalents for the fluid velocity Eq. (3b) are displayed. When $n = |\nabla h_0| = 0$, Eq. (3b) becomes $\partial\mathbf{u}/\partial t = \alpha\nabla(\nabla\cdot\mathbf{u})$, a diffusion equation for the velocity, hence $\alpha > 0$ acts similar to a viscosity. Previous works [13–16] have neglected exchange dispersion and nonlinearity in Eqs. (3) by assuming the long-wavelength, near saturation density, low-velocity limit, i.e., $|\nabla n| \ll 1$, $|n| \ll 1$, and $|\mathbf{u}|^2 \ll 1$. As we show below, the full nonlinearity and exchange dispersion included in Eqs. (3a) and (3b) are required to describe the existence and stability regions of magnetic hydrodynamic states and broken Galilean invariance.

Insight can be gained from the homogeneous field $\nabla h_0 \to 0$, conservative $\alpha \to 0$ limit, where Eqs. (3) become conservation laws for n and $\mathbf{u}$. Notably, the non-negative deviation from vacuum $(1-n^2)$, or *fluid density*, is not conserved. A conservation law for the momentum $\mathbf{p} = n\mathbf{u}$ can also be obtained

$$\begin{aligned}\frac{\partial \mathbf{p}}{\partial t} = {} & \nabla\cdot[(1-n^2)\mathbf{u}\mathbf{u}^T] + \nabla P(n,|\mathbf{u}|) + \nabla\cdot\left[\frac{\nabla n \nabla n^T}{1-n^2}\right] \\ & - \nabla\left[\frac{n\Delta n + \frac{1}{2}|\nabla n|^2}{1-n^2} + \frac{n^2|\nabla n|^2}{(1-n^2)^2}\right],\end{aligned} \tag{5}$$

where the magnetic pressure is defined as

$$P(n,|\mathbf{u}|) = \frac{1}{2}(1+n^2)(\sigma - |\mathbf{u}|^2) - \sigma. \tag{6}$$

Equations (3a) with $\alpha = 0$, and (5) are analogous to the time-reversed Euler equations expressing conservation of mass and momentum for a 2D, compressible, isentropic fluid with a density- and velocity-dependent pressure P.

Additionally, the one-dimensional conservative limit of Eqs. (3a) and (3b) are exactly the equations describing polarization waves in two-component spinor Bose gases [33, 34] and, in the near vacuum ($|n| \sim 1$), long-wavelength, and low-frequency regime, approximate the mean field dynamics of a BEC [24, 42]. This suggests that thin film ferromagnets are ripe for the exploration of nonlinear structures observed in BECs, e.g., "Bosenovas" [25, 27] in attractive ($\sigma = -1$); and dark solitons [30], vortices [22], and DSWs [20] in repulsive ($\sigma = +1$) BECs. Some of these structures have been observed in uniaxial (dissipative droplets [5–7]) and planar (vortices [8]) thin film ferromagnets. As we demonstrate, hydrodynamic states are also supported.

Consider an ideal planar thin film ferromagnet ($\sigma = +1$) and a homogeneous field. Equations (3) admit a static ($\partial\Phi/\partial t = 0$) solution *with nonzero fluid velocity*, $\mathbf{u} = u\hat{\mathbf{x}}$, $|u| < 1$, $n = 0$, and $h_0 = 0$. These are ground states known as spin-density waves (SDWs) [43] or soliton lattices [15] that minimize both exchange and anisotropy energies, i.e., any configuration with $|u| < 1$ is stable when $\mathbf{m}$ lies purely in-plane. SDWs exhibit a periodic structure that affords them topological stability whereby the phase rotation can be unwound only by crossing a magnetic pole ($|n| = 1$) [15, 37]. For a non-zero field, $|h_0| < 1 - u^2$, SDWs are also supported for any $|u| < 1$ when $n = h_0/(1 - u^2)$ due to the longitudinal spin density relaxation effected by Eq. (3a). Such a relaxation maintains u and thus *the topology of and finite spin current carried by* a SDW. This property is identical to that of equilibrium transverse spin currents in other magnetic textures including domain walls and vortices [Ref. 15, Eq. (4) in Ref. 44].

For no damping, Eqs. (3) admit dynamic solutions parametrized by the constants $(\bar{n}, \bar{u})$, where $|\bar{n}| \leq 1$, $\mathbf{u} = \bar{u}\hat{\mathbf{x}}$, called *uniform hydrodynamic state* (UHS). The fluid velocity $\bar{u}$ is the wavenumber of the UHS whose frequency $\Omega = d\Phi/dt$ is

$$\Omega(\bar{n}, \bar{u}) = -(1 - \bar{u}^2)\bar{n} + h_0, \tag{7}$$

obtained from the magnetic equivalent of Bernoulli's equation $2P(\bar{n}, |\bar{u}|) + \bar{u}^2 + \bar{n}(\Omega - h_0) = -\sigma$ [37]. Here, positive $\bar{u}$ implies clockwise *spatial* increase of the azimuthal phase Φ whereas negative Ω implies clockwise *temporal* precession about the $+\hat{\mathbf{z}}$ axis defining forward and

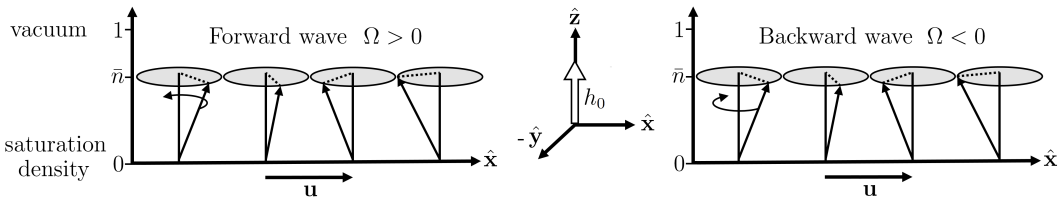


FIG. 1. Schematic of a UHS. The longitudinal spin density is the vertical axis limited by vacuum ($|n| = 1$) and saturation density ($n = 0$). Forward and backward wave conditions are determined by the sign of the frequency Ω.

backward wave conditions, schematically shown in Fig. 1. This is in contrast to magnetostatic forward and backward volume waves established by the relative direction between their wave vector and the external applied field.

The magnetization in a UHS can exhibit large angle deviations from the $+\hat{\mathbf{z}}$ axis, making it a strongly nonlinear texture. Near saturation density, $|\bar{n}| \ll 1$, a UHS limits to a spin superflow [14–16] whereas near vacuum, $\bar{n} \sim \pm 1$, the UHS frequency Eq. (7) becomes the exchange spin-wave dispersion $\Omega \sim \pm\bar{u}^2 + h_0 \mp 1$. Thus, a UHS is the generalization of periodic magnetic textures from large (spin superflow) to small (spin-wave) amplitudes. It is important to recognize that the ground state for the UHS is a SDW, i.e., the ground state of planar ferromagnets is not defined by a single orientation except for the vacuum state. In this sense, the UHS is significantly different from the conventional theory of spin waves based on the Holstein-Primakoff transformation [45] and their strongly nonlinear dynamics. [10, 11].

Small-amplitude perturbations of a UHS can be regarded as spin waves with a generalized dispersion relation obtained from the linearization of Eqs. (3a) and (3b)

$$\omega_\pm(\mathbf{k}, \mathbf{V}) = (2\bar{n}\mathbf{u} - \mathbf{V}) \cdot \mathbf{k} \pm |\mathbf{k}| \sqrt{(1 - \bar{n}^2)(1 - \bar{u}^2) + |\mathbf{k}|^2}, \tag{8}$$

where $\mathbf{k}$ is the wave vector, and the velocity $\mathbf{V}$ reflects a Doppler shift, i.e., the velocity of an external observer with respect to the UHS. The dispersion relation shows that magnetic systems *lack Galilean invariance*. In other words, an observer velocity $\mathbf{V} \propto \mathbf{u}$ does not generally result in a reference frame where the relative fluid velocity is zero. Galilean invariance is recovered near vacuum with dispersion $\omega_\pm(\mathbf{k}, \mathbf{V}) = (2\mathbf{u} - \mathbf{V}) \cdot \mathbf{k} \pm |\mathbf{k}|^2$, i.e. exchange-mediated spin waves and the BEC limit [24, 42]; and for spin superflow, $\omega_\pm(\mathbf{k}, \mathbf{V}) = -\mathbf{V} \cdot \mathbf{k} \pm |\mathbf{k}| \sqrt{1 + |\mathbf{k}|^2}$. More importantly, the fluid velocity $\bar{u}$ confers a spec-

tral *shift* in Eq. (8) due to the UHS's intrinsically chiral topology, similar to interfacial Dzyaloshinskii-Moriya interaction [46].

The long wavelength limit of Eq. (8) leads to coincident spin-wave phase and group velocities, i.e., magnetic sound velocities

$$s_{\pm} = 2\bar{n}\bar{u} + \bar{V} \pm \sqrt{(1-\bar{n}^2)(1-\bar{u}^2)}. \tag{9}$$

Here, we assume $\mathbf{V}$ collinear and opposite to $\mathbf{u}$ ($\mathbf{V} = -\bar{V}\hat{\mathbf{x}}$). Subsonic flow occurs when spin waves can propagate both forward and backward: $s_- < 0 < s_+$. However, when $0 < s_- < s_+$, the flow is supersonic and some spin waves are convected away. These conditions can be quantified in terms of the Mach numbers M_u, M_V when $\bar{V} = 0$, $\bar{u} = 0$, respectively

$$\mathrm{M}_u = |\bar{u}|\sqrt{\frac{1+3\bar{n}^2}{1-\bar{n}^2}}, \quad \mathrm{M}_V = \frac{|\bar{V}|}{\sqrt{1-\bar{n}^2}}. \tag{10}$$

For both, the flow is subsonic or laminar when $\mathrm{M} < 1$. In the supersonic regime, $\mathrm{M} > 1$, it is energetically favorable to generate spin waves, thus leading to the Landau breakdown of superfluid-like flow [47]. The resulting phase diagrams are shown in Fig. 2. Interestingly, Eq. (10) predicts that M is independent of h_0, implying that only the UHS longitudinal spin density and its non-trivial topology, $\bar{u}$, set the supersonic transition, not the frequency Ω. It must be noted that broken Galilean invariance causes the Landau criterion concept $\bar{u} < \min[s_{\pm}]$ [24] to give an incorrect sonic curve.

A qualitatively distinct flow regime occurs when $|\bar{u}| > 1$ and the sound velocities Eq. (9) are complex. This corresponds to a change in the mathematical type of the long wavelength Eqs. (3) from hyperbolic (wave-like) to elliptic (potential-like). Consequently, the UHS is unstable in the sense that small fluctuations lead to drastic changes in its temporal evolution or modulational instability (MI) [48, 49]. Note that $|\bar{u}| < 1$, $|\bar{V}| > 1$ does not result in MI.

The aforementioned regimes were validated by performing micromagnetic simulations with damping [12]. We simulate dynamics for an ideal Permalloy nanowire ($\mu_0 M_s = 1$ T) of nondimensional width $w = 20$ with transverse free spin boundary conditions and horizontal periodic boundary conditions (PBCs). We initialize with a SDW, include only local dipolar fields (zero thickness limit), and set $\alpha = 0.01$. A homogeneous field h_0 stabilizes the SDW at a specific $\bar{n}$ and a quantized $\bar{u}$ that satisfies the PBC. This enables us to numerically probe along a horizontal line in the phase diagram of Fig. 2(a) by implementing a slowly increasing h_0. By inserting a point defect (a magnetic void), the SDW spontaneously generates spin

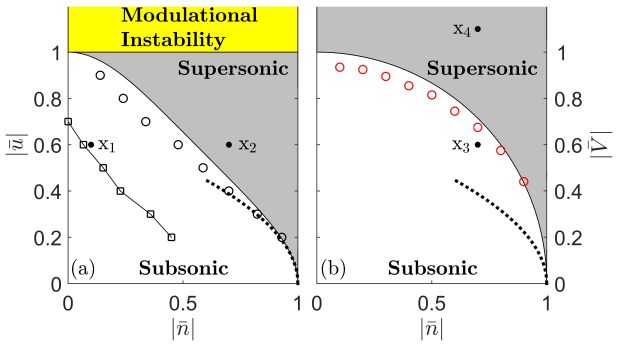


FIG. 2. UHS phase diagram for (a) $\bar{V} = 0$ and (b) $\bar{u} = 0$ with subsonic (white), supersonic (gray), and modulationally unstable (yellow) regimes. Circles are numerical estimates of the sonic curves $\mathrm{M}_u = 1$ and $\mathrm{M}_V = 1$. The BEC regime sonic curve is dashed. Open squares represent the sonic curve of a width $w = 20$, thickness $\delta = 1$ nanowire including non-local dipolar fields and $T = 300$ K thermal field. Selected simulation conditions are denoted by x_1 to x_4.

waves when $\bar{n}$ is large enough to cross the supersonic transition, leading to a breakdown in the spatial homogeneity of the SDW [37]. Due to the SDW's topology and the PBC, the change in symmetry is accommodated by annihilating a single 2π phase rotation and reducing $\bar{u}$ in a quantized fashion. Topologically, this is possible in planar ferromagnets by crossing a magnetic pole, e.g., nucleating a vortex, as shown in the Supplementary Video 1. This was also observed in wires of width $w = 40$. The sonic curve estimated this way is shown in Fig. 2(a) by black circles, demonstrating good agreement with $\mathrm{M}_u = 1$. We attribute any discrepancy to boundary and finite size effects [50], as further explored below.

We use the same numerical method described above with the addition of thermal fluctuations and the symmetry-breaking non-local dipolar fields to study the stability of a SDW in a nanowire of nondimensional thickness $\delta = 1$. In this case, the SDW topological structure completely collapses at the boundary shown in Fig. 2(a) by squares. In contrast to a recent report where stable spin superflow was predicted only for nanowires shorter than the material exchange length [18], we observe stable SDWs over a wide range of parameters in phase space (Supplementary Video 2).

The supersonic transition in the moving frame is estimated by use of a numerical method described elsewhere [51]. A moving, perpendicular, localized, weak magnetic field spot with velocity $\bar{V}$ is used to perturb a homogeneous state in the bias field $h_0 = \bar{n}$. The obtained

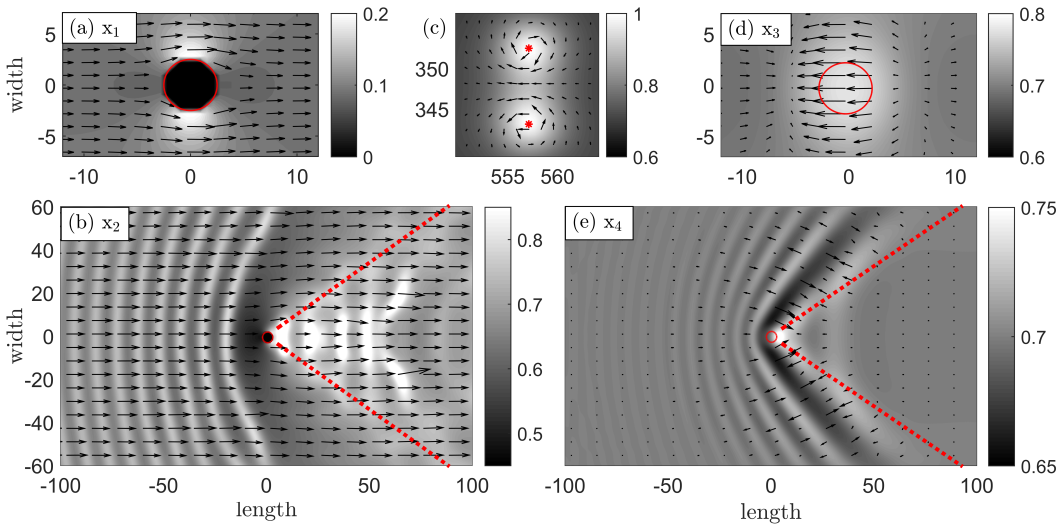


FIG. 3. Snapshots of a (a), (b) SDW flowing past a stationary magnetic defect ($\bar{V} = 0$) and; (d), (e) a homogeneous state subject to a moving, localized magnetic field ($\bar{V} \neq 0$) with longitudinal spin density n (grayscale map) and velocity field $\mathbf{u}$ (arrows). The simulation region is much larger than what is visible. The defect or localized magnetic field position is shown by a red circle. For subsonic conditions, (a) and (d), the flow is static and laminar. In supersonic flow, (b) and (e), a Mach cone (dashed) and static wavefronts are observed. Propagating vortex-antivortex pairs with cores (asterisks) generated in (b) are shown in (c) far from the defect as opposite circulations of the velocity field (background $\bar{u} = 0.6$ subtracted).

sonic curve is in good agreement with $\mathrm{M}_V = 1$, shown in Fig. 2(b) by red circles.

We now explore the effect of finite-sized obstacles on a UHS. As observed in BECs, obstacles can generate vortices, wavefronts, and DSWs in a fluid flow [20–22]. Note that wavefronts, i.e., "spin-Cerenkov" radiation, were previously observed via micromagnetic simulations in homogeneous ($\bar{u} = 0$), thick ferromagnets in the moving reference frame ($\bar{V} \neq 0$) [52]. The wavefronts studied here are different, resulting from both moving ($\bar{u} = 0$, $\bar{V} \neq 0$) and static ($\bar{u} \neq 0$, $\bar{V} = 0$) reference frames; yet another manifestation of broken Galilean invariance. We illustrate these features with simulations where $\alpha = 0.01$ and local dipolar fields are included, shown in Fig. 3 as a grayscale map and vector field for n and $\mathbf{u}$, respectively [see Supplement for the corresponding in-plane magnetization map]. First, we consider the subsonic conditions x_1 of Fig. 2(a) for a SDW in the static reference frame $(\bar{n}, \bar{u}) = (0.1, 0.4)$ with a magnetic defect within a circular area of $\pi/\bar{u}$ in diameter. The

static configuration in Fig. 3(a) is analogous to Bernoulli's principle for laminar flow.

A different situation occurs at supersonic conditions x_2 $(\bar{n}, \bar{u}) = (0.7, 0.6)$, Fig. 3(b). Here, the density develops a distinct Mach cone (dashed), delimiting static wavefronts and the nucleation of propagating vortex-antivortex pairs, shown far from the defect in Fig. 3(c). In the moving reference frame, a homogeneous state is perturbed by a moving, weak, localized field. Utilizing the subsonic conditions x_3 $(\bar{n}, \bar{u}, \bar{V}) = (0.7, 0, 0.6)$, the flow is laminar, Fig. 3(d) [c.f. supersonic x_2 in Fig. 2(a)]. Wavefront radiation outside the Mach cone is observed for the supersonic condition x_4 $(\bar{n}, \bar{u}, \bar{V}) = (0.7, 0, 1.1)$ in Fig. 3(e). However, the field spot amplitude is too weak to excite vortex-antivortex pairs. Animations are in Supplementary Videos 3 to 6.

The MI regime for UHSs with $|\bar{u}| > 1$ exhibits a violent instability (see Supplementary Video 7). Notably, for a uniaxial ferromagnet with $\sigma = -1$, MI is always operative. This is consistent with the focusing of spin waves and the formation of dissipative droplets in spin torque devices utilizing materials with perpendicular magnetic anisotropy [4–7].

We now discuss an experimental test for the hydrodynamic predictions. As mentioned above, the dispersion relation Eq. (8) features a spectral shift with non-zero fluid velocity. This shift can be observed e.g., by means of Brillouin light scattering (BLS), as already shown for Dzyaloshinskii-Moriya interactions [46]. For a given fluid velocity, the magnitude of the shift, $2\bar{n}\bar{u}$, can be tuned by an externally applied field. Use of such tuning, in combination with BLS, will allow a direct test of the predicted breaking of Galilean invariance, insofar as the nonlinear properties of the dispersion relation Eq. (8) can be quantitatively investigated. In particular, if one plots spin-wave frequency vs. wavenumber squared for both the Stokes and anti-Stokes BLS peaks in the short-wavelength limit, $|\mathbf{k}| \gg (1-\bar{n}^2)(1-\bar{u}^2)$, the modulus of the zero-wavenumber intercepts from linear regression *will not be equal in the case of broken Galilean invariance*, in contrast to the case of Galilean invariance, where the intercepts should be equal.

In summary, the dispersive hydrodynamic (DH) formulation permits us to quantify the manner in which thin film ferromagnets lack Galilean invariance in the context of linear spin wave propagation on a dynamic UHS or static SDW background. The breaking of Galilean invariance is often associated with relativistic phenomena wherein the Lorentz transformation conjoins space-time into a single coordinate system, replacing the Galilean transformation. Instead, the present case ultimately reflects the counterintuitive ability of

exchange-coupled, topological spin textures to support spin currents, even in the static case. The predictions are robust to damping, non-local dipolar fields, and finite temperatures for a large portion of phase space. The exact representation of the LL equation in DH form along with associated mathematical tools [23, 31, 48] enables new magnetodynamic predictions and a frontier of magnetic research, for example the observation of a Mach cone, wavefronts, and vortex nucleation, suggesting the existence of coherent structures such as oblique solitons and DSWs.

ACKNOWLEDGMENTS

The authors thank Leo Radzihovsky for beneficial discussions. E.I. acknowledges support from the Swedish Research Council, Reg. No. 637-2014-6863. M.A.H. partially supported by NSF CAREER DMS-1255422.

[1] L. Berger, Phys. Rev. B **54**, 9353 (1996).

[2] J. C. Slonczewski, J. Magn. Magn. Mater. **159**, L1 (1996).

[3] K. M. D. Hals and A. Brataas, Phys. Rev. B **88**, 085423 (2013).

[4] M. A. Hoefer, T. J. Silva, and M. W. Keller, Phys. Rev. B **82**, 054432 (2010).

[5] S. M. Mohseni, S. R. Sani, J. Persson, T. N. A. Nguyen, S. Chung, Y. Pogoryelov, P. K. Muduli, E. Iacocca, A. Eklund, R. K. Dumas, S. Bonetti, A. Deac, M. A. Hoefer, and J. Åkerman, Science **339**, 1295 (2013).

[6] F. Macià, D. Backes, and A. Kent, Nature Nanotechnol **10**, 1038 (2014).

[7] S. Chung, A. Eklund, E. Iacocca, S. Mohseni, S. Sani, L. Bookman, M. A. Hoefer, R. Dumas, and J. Åkerman, Nature Communications **7** (2016).

[8] Q. Mistral, M. van Kampen, G. Hrkac, J.-V. Kim, T. Devolder, P. Crozat, C. Chappert, L. Lagae, and T. Schrefl, Phys. Rev. Lett. **100**, 257201 (2008).

[9] A. Slavin and V. Tiberkevich, Magnetics, IEEE Transactions on **45**, 1875 (2009).

[10] V. L'vov, *Wave turbulence under parametric excitation* (Springer, 1994).

[11] G. Bertotti, I. Mayergoyz, and C. Serpico, *Nonlinear magnetization dynamics in nanosystems*, first edition ed. (Elsevier Science, 2008).

[12] A. Vansteenkiste, J. Leliaert, M. Dvornik, M. Helsen, F. Garcia-Sanchez, and B. Van Waeyenberge, AIP Advances **4**, 107133 (2014).

[13] B. Halperin and P. Hohenberg, Physical Review **188**, 898 (1969).

[14] J. König, M. C. Bønsager, and A. H. MacDonald, Phys. Rev. Lett. **87**, 187202 (2001).

[15] E. B. Sonin, Advances in Physics **59**, 181 (2010).

[16] S. Takei and Y. Tserkovnyak, Phys. Rev. Lett. **112**, 227201 (2014).

[17] H. Chen, A. D. Kent, A. H. MacDonald, and I. Sodemann, Phys. Rev. B **90**, 220401 (2014).

[18] H. Skarsvåg, C. Holmqvist, and A. Brataas, Phys. Rev. Lett. **115**, 237201 (2015).

[19] B. Flebus, S. A. Bender, Y. Tserkovnyak, and R. A. Duine, Phys. Rev. Lett. **116**, 117201 (2016).

[20] M. A. Hoefer, M. J. Ablowitz, I. Coddington, E. A. Cornell, P. Engels, and V. Schweikhard, Phys. Rev. A **74**, 023623 (2006).

[21] I. Carusotto, S. X. Hu, L. A. Collins, and A. Smerzi, Phys. Rev. Lett. **97**, 260403 (2006).

[22] A. L. Fetter, Reviews of Modern Physics **81**, 647 (2009).

[23] G. El and M. Hoefer, Physica D, to appear (2016).

[24] C. Pethick and H. Smith, *Bose-Einstein condensation in dilute gasses* (Cambridge University Press, 2002).

[25] E. A. Donley, N. R. Claussen, S. L. Cornish, J. L. Roberts, E. A. Cornell, and C. E. Wieman, Nature **412**, 295 (2001).

[26] G. A. El, A. Gammal, and A. M. Kamchatnov, Phys. Rev. Lett. **97**, 180405 (2006).

[27] S. L. Cornish, S. T. Thompson, and C. E. Wieman, Physical Review Letters **96**, 170401 (2006).

[28] Y. G. Gladush, G. A. El, A. Gammal, and A. M. Kamchatnov, Phys. Rev. A **75**, 033619 (2007).

[29] P. G. Kevrekidis, D. J. Frantzeskakis, and R. Carretero-Gonzàlez, *Emergent nonlinear phenomena in Bose-Einstein condensates: theory and experiment* (Springer, Berlin, 2008).

[30] D. J. Frantzeskakis, Journal of Physics A: Mathematical and Theoretical **43**, 213001 (2010).

[31] P. G. Kevrekidis, D. J. Frantzeskakis, and R. Carretero-González, *The Defocusing Nonlinear Schrödinger Equation* (SIAM, Philadelphia, 2015).

[32] S. Demokritov, V. Demidov, O. Dzyapko, G. A. Melkov, A. A. Serga, B. Hillebrands, and A. Slavin, Nature **443**, 430 (2006).

[33] C. Qu, L. P. Pitaevskii, and S. Stringari, Phys. Rev. Lett. **116**, 160402 (2016).

[34] T. Congy, A. M. Kamchatnov, and N. Pavloff, arXiv:1607.08760 (2016).

[35] G. Beach, M. Tsoi, and J. Erskine, Journal of Magnetism and Magnetic Materials **320**, 1272 (2008).

[36] K. Yamada, S. Kasai, Y. Nakatani, K. Kobayashi, H. Kohno, A. Thiaville, and T. Ono, Nature **6**, 269 (2007).

[37] See Supplementary Material [url], which includes Refs. [53-54].

[38] S. K. Kim, S. Takei, and Y. Tserkovnyak, Phys. Rev. B **92**, 220409 (2015).

[39] N. Papanicolaou and T. Tomaras, Nuclear Physics B **360**, 425 (1991).

[40] S. Zhang and Z. Yang, Phys. Rev. Lett. **94**, 066602 (2005).

[41] A. Hoffmann, IEEE Advances on magnetics **49**, 5172 (2013).

[42] I. I. Satija and R. Balakrishnan, Phys. Lett. A **375**, 517 (2011).

[43] G. Grüner, Rev. Mod. Phys. **66**, 1 (1994).

[44] Y. Tserkovnyak, E. M. Hankiewicz, and G. Vignale, Phys. Rev. B **79**, 094415 (2009).

[45] D. C. Mattis, *The theory of magnetism made simple* (World Scientific publishing, Hackensack, NJ, 2006) pp. 82–103.

[46] H. T. Nembach, J. M. Shaw, M. Weller, E. Jué, and T. J. Silva, Nature Physics **11**, 825 (2015).

[47] L. D. Landau, J. Phys. USSR **5**, 71 (1941).

[48] G. B. Whitham, *Linear and nonlinear waves* (John Wiley & Sons Inc, 1974).

[49] V. Zakharov and L. Ostrovsky, Physica D **238**, 540 (2009).

[50] T. Frisch, Y. Pomeau, and S. Rica, Physical Review Letters **69**, 1644 (1992).

[51] M. Hoefer and M. Sommacal, Physica D: Nonlinear Phenomena **241**, 890 (2012).

[52] M. Yan, A. Kákay, C. Andreas, and R. Hertel, Phys. Rev. B **88**, 220412 (2013).

[53] M. Sparks, *Ferromagnetic relaxation theory* (McGraw-Hill, 1965).

[54] H.-B. Braun, Advances in Physics **61**, 1 (2012).

SUPPLEMENTARY MATERIAL

I. NONDIMENSIONALIZATION OF THE LANDAU-LIFSHITZ EQUATION

The Landau-Lifshitz (LL) equation can be written as

$$\frac{\partial \mathbf{M}}{\partial t} = -\frac{\gamma \mu_0}{1+\alpha^2}\left[\mathbf{M}\times\mathbf{H}_{\text{eff}} + \frac{\alpha}{M_s}\mathbf{M}\times(\mathbf{M}\times\mathbf{H}_{\text{eff}})\right], \tag{11}$$

where the damping α is in Gilbert form, $\mathbf{M}$ is the magnetization vector, $M_s = |\mathbf{M}|$ is the saturation magnetization, γ is the gyromagnetic ratio, μ_0 is the vacuum permeability, and the effective field is

$$\mathbf{H}_{\text{eff}} = \lambda_{\text{ex}}^2 M_s \Delta \mathbf{m} + M_{\text{eff}}(\mathbf{m}\cdot\hat{\mathbf{z}})\hat{\mathbf{z}} + H_0\hat{\mathbf{z}}, \tag{12}$$

where $\mathbf{m} = \mathbf{M}/M_s$, $\lambda_{\text{ex}} = \sqrt{2A/(\mu_0 M_s^2)}$ is the exchange length, A is the exchange constant with units Jm^{-1}, $M_{\text{eff}} = (2K_u/(\mu_0 M_s) - M_s)$, and K_u is the perpendicular magnetic anisotropy energy density with units Jm^{-3}. In order to generalize our results for materials favoring either planar or uniaxial anisotropy, we introduce the quantity $\sigma = \text{sgn}(M_s - H_k)$, where $H_k = 2K_u/(\mu_0 M_s)$ is the perpendicular magnetic anisotropy field. It is then possible to rescale time $t \to \gamma\mu_0|H_k - M_s|(1+\alpha^2)^{-1}t$, space $x \to \sqrt{|H_k/M_s - 1|}\lambda_{ex}^{-1}x$, and field $h_{\text{eff}} = H_{\text{eff}}/|H_k - M_s|$. As a result, we obtain the dimensionless Landau-Lifshitz equation

$$\frac{\partial \mathbf{m}}{\partial t} = -\mathbf{m}\times\mathbf{h}_{\text{eff}} - \alpha\mathbf{m}\times\mathbf{m}\times\mathbf{h}_{\text{eff}}, \tag{13}$$

[Eq. (1) in the main text]. Note that the special case of an isotropic ferromagnet $H_k = M_s$ leads to a divergence from our nondimensionalization. However, we consider that an isotropic thin film ferromagnet is experimentally unlikely, in which case the divergence does not affect the generality of the analytical results.

II. DERIVATION OF HYDRODYNAMIC EQUATIONS

The dispersive hydrodynamic representation can be derived by inserting the canonical Hamiltonian transformation

$$n = m_z, \tag{14a}$$

$$\mathbf{u} = -\nabla\Phi = -\nabla\left[\arctan\left(m_y/m_x\right)\right], \tag{14b}$$

into Eq. (13). Solving for $\partial\Phi/\partial t$ we obtain the exact transformation

$$\frac{\partial\Phi}{\partial t} = -(\sigma - |\mathbf{u}|^2)n + \frac{\Delta n}{1-n^2} + \frac{n|\nabla n|^2}{(1-n^2)^2} + h_0 - \frac{\alpha}{1-n^2}\nabla\cdot[(1-n^2)\mathbf{u}]. \tag{15}$$

Solving for $\partial n/\partial t$ and $\partial\mathbf{u}/\partial t = -\nabla\partial\Phi/\partial t$ we obtain

$$\frac{\partial n}{\partial t} = \nabla\cdot\left[(1-n^2)\mathbf{u}\right] + \alpha(1-n^2)\frac{\partial\Phi}{\partial t}, \tag{16a}$$

$$\frac{\partial\mathbf{u}}{\partial t} = \nabla\left[(\sigma - |\mathbf{u}|^2)n\right] - \nabla\left[\frac{\Delta n}{1-n^2} + \frac{n|\nabla n|^2}{(1-n^2)^2}\right] - \nabla h_0 + \alpha\nabla\left[\frac{1}{1-n^2}\nabla\cdot\left[(1-n^2)\mathbf{u}\right]\right]. \tag{16b}$$

Interpreting n as the longitudinal spin density, we observe that Eq. 16a is reminiscent of the continuity equation [40] in the absence of damping

$$\frac{\partial\mathbf{M}\cdot\hat{\mathbf{z}}}{\partial t} = -\nabla\cdot\mathbf{J}_s + T + T_{\text{relax}}, \tag{17}$$

where $\mathbf{J}_s$ is the spin current, T is spin torque, and T_{relax} is a relaxation process. Therefore, we identify the first term of the right-hand-side of Eq. (16a) as the spin current, acknowledging the sign difference arising from our definition of $\mathbf{u}$.

The term $(1-n^2)$ appearing in Eq. (16a) is non-negative, quantifying the fluid density deviation from vacuum, $|n| = 1$. However, one can verify that this is not a conserved quantity. In fact, neglecting damping,

$$\frac{\partial(1-n^2)}{\partial t} = 2n\frac{\partial n}{\partial t} = 2n\nabla\cdot\left[(1-n^2)\mathbf{u}\right], \tag{18}$$

whose right-hand-side cannot be written as a divergence. This agrees with the notion that spin current itself is not a conserved quantity even when damping is zero, whereas the longitudinal spin density is always conserved [40] in the absence of specific processes. Indeed, this is a restatement of the fact that spin currents in ferromagnets have both a coherent and diffusive character, where the coherent form is typified by spin wave propagation, whereas the diffusive character is associated with thermal magnon kinetics. As such, the lack of conservation for the fluid density in ferromagnets is analogous to the fact that the energy-conserving coherence lifetime τ_2 in the Bloch formulation of spin dynamics can be substantially shorter than the thermodynamic relaxation time τ_1 [53].

In the long-wavelength, low-frequency, near saturation density limit, $|\nabla n| \ll 1$, $|\mathbf{u}|^2 \ll 1$, and $n \ll 1$, we obtain

$$\frac{\partial n}{\partial t} = -\Delta\Phi + \alpha\frac{\partial \Phi}{\partial t}, \tag{19a}$$

$$\frac{\partial \Phi}{\partial t} = -\sigma n + h_0 + \alpha\Delta\Phi. \tag{19b}$$

These equations are consistent with the equations describing spin superfluidity [15, 16].

Considering a UHS with a uniform precessional frequency $d\Phi/dt = \Omega$, no damping, and neglecting spatial variation in n, the magnetic analogue of Bernoulli's equation can be obtained by multiplying Eq. (15) by $n/2$

$$P(n, |\mathbf{u}|) + \frac{1}{2}|\mathbf{u}|^2 + \frac{1}{2}n(\Omega - h_0) = -\frac{\sigma}{2}, \tag{20}$$

where P is pressure, the second term is the kinetic energy, the third term is a potential (analogous to gravity).

III. MICROMAGNETIC SIMULATIONS

We perform micromagnetic simulations to validate our analytical results. For the magnetic defect in the static frame, $\mathbf{V} = 0$, we use the GPU-accelerated code Mumax3 [12]. In order to maintain a SDW in the absence of external forcing, e.g., spin injection, we set a SDW with an integer number of periods as an initial magnetization state and implement periodic boundary conditions (PBC) along the nanowire's length and free spin boundary conditions transversely. The integer period requirement sets the length of the simulation area. We use idealized physical parameters consistent with infinitely permeable Permalloy, $M_s = 790$ kA/m, $A = 10$ pJ/m, and $H_k = 0$. In this case, space is normalized by $\lambda_{\text{ex}} \approx 5$ nm according to the nondimensionalization introduced above. Three types of simulations were performed:

1. To estimate the sonic curve, we set a nanowire of 20 in width, $20\pi/\bar{u}$ in length, and 1 in thickness. A SDW at a particular $\bar{u}$ is defined as an initial condition. Taking advantage of the field relaxation of the longitudinal spin density, we set $\alpha = 0.01$ and sweep the field at a normalized rate of 1×10^{-5} (on the order of 0.3 T/μs). This rate is slow enough to sweep $\bar{n}$ as a function of field. A point-defect is introduced as an absence of magnetization. The supersonic condition is obtained at the point when

the linear increase in $\bar{n}$ changes slope, corresponding to a quantized drop of the SDW topological charge.

2. The supersonic transition is also estimated by including non-local dipolar fields. In contrast to case 1 above, we do not consider any defect and instead add room temperature (300 K) thermal fluctuations. The supersonic transition is identified as a dramatic drop in the longitudinal spin density $n = m_z$, corresponding to the generation of spin wave as the UHS decays. To take into account the noise introduced by thermal fluctuations, a linear fit is applied to the averaged m_z. The error is obtained from the standard deviation throughout the simulation time.

3. The effect of finite-sized obstacles is obtained from simulations on a domain spanning 640 in width, 640 in length, and 1 in thickness. We set the damping to $\alpha = 0.01$ and utilize an external field to maintain the desired longitudinal spin density. This size guarantees that the generated features damp before reaching the simulation physical boundary.

In the case of the moving obstacle, a localized applied field spot, we use a pseudo-spectral method to solve the two-dimensional Landau-Lifshitz equation in the moving frame [51]. The simulation is initialized with an homogeneous state, $\mathbf{u} = 0$. The localized field spot magnitude is set to 0.05 in normalized units. Two types of simulations are performed:

1. To estimate the sonic curve, we set a simulation area of 100 in width and 80 in length. A point-field is implemented as a hyper-Gaussian of order 4 and width 1. Transient structures are damped during the simulation time. Thus, the supersonic transition is estimated by the existence of a well-defined wave front, i.e., wavefront radiation.

2. The effect of finite-sized obstacles is obtained from a simulation following the geometry described in point 3 above.

IV. FLUID-LIKE BEHAVIOR FOR THE IN-PLANE MAGNETIZATION

In the main text, Fig. 3 shows the fluid-like behavior of a thin film planar ferromagnet, both in the static and moving reference frames. A hydrodynamic visualization is chosen, where the longitudinal spin density n and fluid velocity $\mathbf{u}$ are represented by a grayscale map

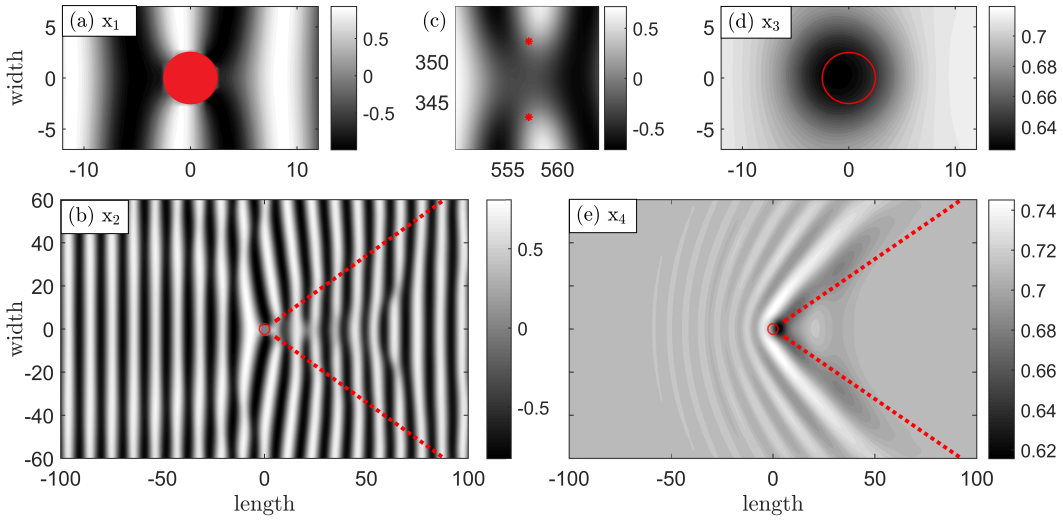


FIG. 4. Snapshots of (a), (b) a SDW flowing past a stationary magnetic defect ($\bar{V} = 0$) and; (d), (e) a homogeneous state subject to a moving, localized magnetic field ($\bar{V} \neq 0$). The grayscale map shows the m_x component and the panels are in exact correspondence with those shown in the main text.

and vector field, respectively. Here, we show the corresponding $\hat{\mathbf{x}}$ magnetization component (m_x) in Fig. 4 as a grayscale map. Note that the SDW, Fig. 4(a-c), is visualized as a periodic variation of m_x. The features arising in the subsonic and supersonic conditions distort this periodic configuration. Notably, the vortex-antivortex, Fig. 4 breaks the periodicity of the SDW. This can be understood by topological arguments, as outlined in the next section. In contrast, the homogeneous state in the moving reference frame exhibits similar features for m_x and n.

V. HYDRODYNAMIC TOPOLOGY

The notion of topology in our hydrodynamic framework is tightly linked to the definition of the magnetic ground state. The concept of topology is typically used to mathematically classify states or textures into groups separated by an infinite barrier (see Ref. 54 for details). Thus, a texture belonging to a certain topological group cannot change its topological group i.e., it is topologically protected. Within a topological group, textures are allowed to be continuously deformed, i.e., such a deformation does not cross a barrier.

Physically, topological barriers correspond to a large, but finite, energy. In a magnetic

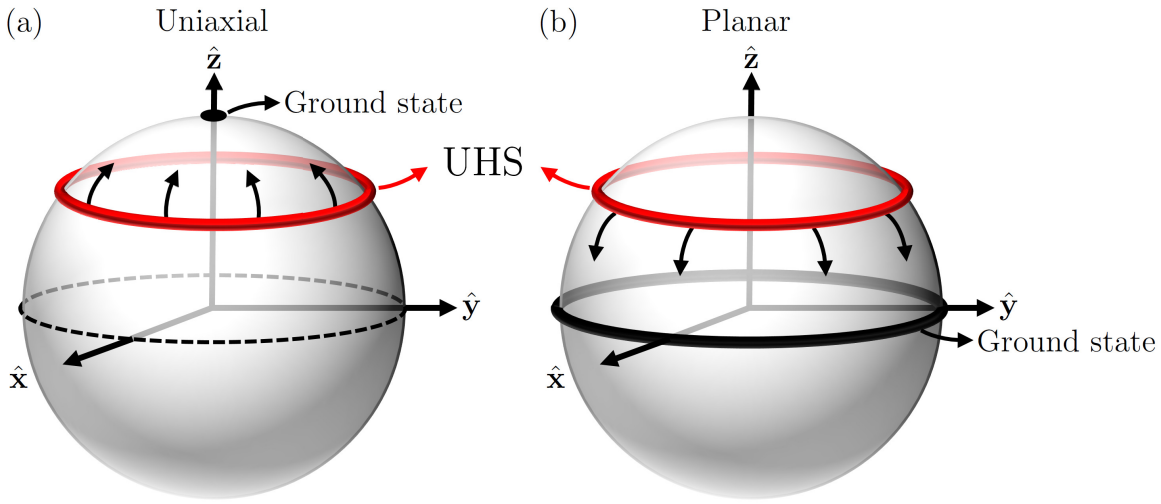


FIG. 5. Relaxation of a UHS in a (a) uniaxial and (b) planar ferromagnet to their ground state. In (a), the UHS can relax to the homogeneous magnetization state whereas in (b) the UHS maintains its phase structure and, therefore, its topology.

system, such a barrier can be interpreted as the magnetization hard axis. For example, a domain wall separating two magnetic states crosses a hard axis, and is therefore topologically protected. In fact, domain walls are usually annihilated by hitting a pinning site or a physical boundary, where the energy barrier can be easily surpassed.

In the hydrodynamic context, we are interested in solutions such as a UHS, exhibiting phase rotations in the $\hat{\mathbf{x}}$-$\hat{\mathbf{y}}$ plane. Therefore, in the magnetization unit sphere, a UHS traces a circle [15]. At this point, it is important to distinguish between uniaxial and planar ferromagnets. For uniaxial ferromagnets, the UHS circle can be continuously deformed along the unit sphere latitude until it reaches its ground state, the $\hat{\mathbf{z}}$ axis. This is schematically shown in Fig. 5(a) for a UHS circle (red) in the northern hemisphere. Consequently, UHSs in uniaxial ferromagnets do not cross the hard axis to return to the homogeneous ground state, $\pm\hat{\mathbf{z}}$, which is typically referred to as a state with trivial topology. It is important to point out that other topological structures are allowed in uniaxial ferromagnets, such as Bloch domain walls, where the ground states are separated by the hard plane.

In the case of planar ferromagnets, the ground state is the isotropic easy plane. Thus, a UHS can continuously deform to a circle along the equator, i.e., a SDW when $h_0 = 0$, as shown in Fig. 5(b). Since this ground state is not homogenous, it possesses a non-trivial topology. For this reason, UHSs in planar ferromagnets exhibit topological protection. The

only mechanism to annihilate a UHS is to cross the hard axis i.e., the $\pm\hat{\mathbf{z}}$ poles. As shown in the Supplementary Video 1, this is achieved by creating a magnetic vortex whose core points exactly along the hard axis and it is therefore an avenue to unwind a phase rotation. From this topological argument, it is also clear that the state with $n = 1$ does not possess topology and it is therefore the hydrodynamic vacuum state.